# Locations of selected small earthquakes in the Zagros mountains

**R. B. Lohman**

*Woods Hole Oceanographic Institution, MS 24, Woods Hole, Massachusetts 02543, USA (rlohman@whoi.edu)*

**M. Simons**

*Seismological Laboratory, California Institute of Technology, Pasadena, California 91125, USA*

[1] The Zagros mountains of southern Iran are marked by a zone of high seismicity and accommodate a significant portion of the convergence between Arabia and Eurasia. Due to the lack of dense local seismic or geodetic networks, the inferred kinematics of the collision in Iran is mainly based on catalogs of teleseismically determined earthquake locations. We surveyed all $M_w > 4.5$ earthquakes in the Harvard Centroid Moment Tensor (HCMT) and International Seismological Centre (ISC) catalogs that occurred in the Zagros mountains during the period 1992–2002 and that were spanned by Interferometric Synthetic Aperture Radar (InSAR) images from the ERS 1 and 2 satellites. We invert the observed deformation for the best fitting point source, single fault plane, and distributed fault slip for four earthquakes and one unexplained deformation event. We find that we can precisely locate earthquakes that are too small to be well-located by either the HCMT or ISC catalogs, allowing us to tie specific earthquakes to active geologic structures.

## 1. Introduction

[2] Much of our understanding of how continental crust accommodates plate tectonic motions comes from studies of the spatial distribution of seismicity in actively deforming mountain belts [e.g., *Jackson and McKenzie*, 1988]. In regions such as the Zagros mountains of southern Iran (Figure 1), which accommodate part of the ~3 cm/yr convergence between Arabia and Eurasia, there are no dense local seismic or geodetic networks and we must rely on catalogs of teleseismically determined earthquake locations. These catalogs have been used both to describe and interpret the spatial distribution of seismically released strain [e.g., *Hessami et al.*, 2001], and to place bounds on the percentage of convergence which is accommodated seismically [e.g., *Jackson and McKenzie*, 1988]. Both of these applications require high-quality estimates of earthquake locations, magnitudes and mechanisms. Catalogs of teleseismically determined earthquake locations in this region commonly have uncertainties of up to 50 km in map view [e.g., *Maggi et al.*, 2000; *Ambraseys*, 2001; *Talebian and Jackson*, 2004] and earthquake depths in the Zagros are poorly determined to the extent that it is difficult to resolve whether earthquakes occur in the basement or in the overlying
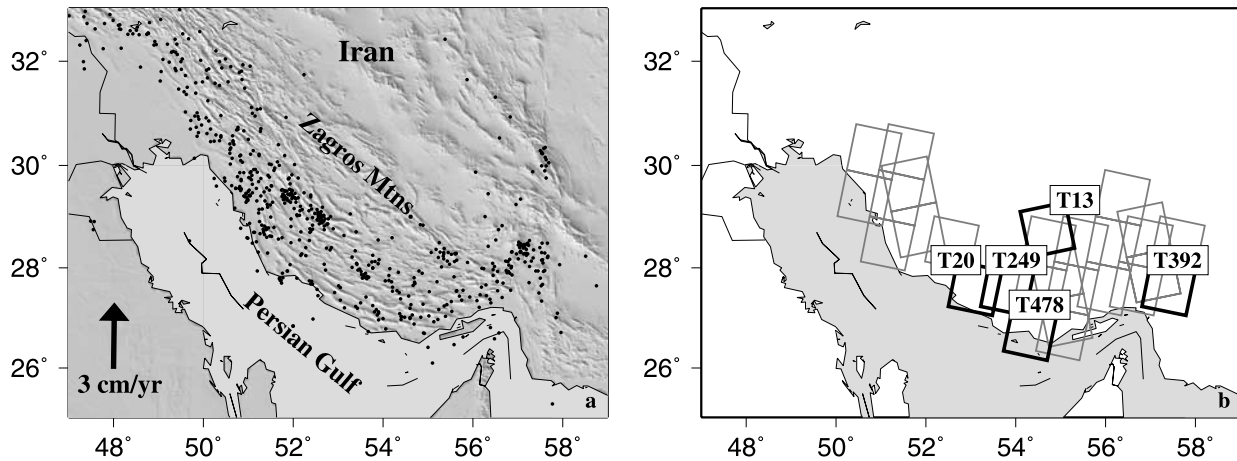
**Figure 1.** (a) Reference map, with shaded topographic relief and seismicity from ISC catalog between 1992 and 2002. Arrow in lower left shows velocity of Arabian plate with respect to Eurasia from the Nuvel-1A model [*DeMets et al.*, 1994]. (b) Gray boxes indicate SAR frames that we examined in this study (some with multiple interferometric pairs); heavy outlines correspond to frames with observed deformation.

10–15 km of sediments [e.g., *Jackson and Fitch*, 1981].

[3] We augment existing seismic catalogs with a set of precise earthquake locations inferred from Interferometric Synthetic Aperture Radar (InSAR) observations. InSAR and seismology are complementary in that InSAR observations are very sensitive to the 3-D location and magnitude of smaller earthquakes, whereas seismology can place strong constraints on the earthquake mechanism [e.g., *Lohman et al.*, 2002].

## 2. Catalog Search

[4] The existing catalog of InSAR data from the ERS 1 and 2 satellites provides sparse temporal and spatial coverage over the Zagros mountains, with the highest data density in the south near the Straits of Hormuz. Since the number of earthquakes in the Harvard Centroid Moment Tensor (HCMT) and International Seismological Centre (ISC) catalogs that occurred in the Zagros between 1992 and 2002 with $M_w > 4.5$ is very large (>500), we implement an automated search procedure that extracts only earthquakes spanned by interferometric pairs with reasonable spatial and temporal baselines (<150 m and <3 years, respectively). From this much smaller family of earthquakes, we hand-checked against known problems with agricultural regions, sand dunes and steep topography. Our final list included 96 potentially detectable earthquakes that are spanned by ~110 interferometric pairs. To process the InSAR data, we used the ROI_PAC software suite [*Rosen et al.*, 2004], and removed topography using the two-pass method [e.g., *Rosen et al.*, 2000] with a 90 m DEM for the region such as is now available from NASA's SRTM mission [*Farr and Kobrick*, 2000].

## 3. Results

[5] We found four regions of localized deformation that we can potentially associate with specific

**Table 1.** Track and Frame for Each Earthquake, With Magnitude and Depth to the Center of the Fault Plane[a]

| Date | T/F | InSAR $M_w$/Z | HCMT $M_w$/Z/Err | ISC $m_b$/Z/Err | N |
|------|-----|---------------|-------------------|------------------|---|
| 97/05/05 | 478/3069 | 5.4/4.4 | 5.0/15/46 | 4.8/46/2 | 1 |
| 97/09/18 | 478/3069 | 5.0/3.5 | - | 4.7/55/4 | 1 |
| 98/10/01 | 13/567 | 4.7/0.7 | - | 4.2/98/11 | 2 |
| 99/04/30 | 20/3051[b] | 5.3/3.2 | 5.1/45/67 | 4.9/35/7 | 3 |
| Unknown | 392/3051 | 4.8/2.0 | N/A | N/A | 2 |

[a] T/F, track and frame for each earthquake; $M_w$, magnitude; Z, depth to the center of the fault plane in kilometers inferred from InSAR data (this paper) and from the HCMT and ISC catalogs; Err, map view location error in kilometers for the HCMT and ISC locations relative to the InSAR-derived locations. N indicates the number of interferograms that show deformation for each earthquake.
[b] Signal also observed in interferograms from an overlapping track.

**Table 2.** InSAR Data Used in This Study

| Track | Frame | Date 1 | Date 2 | $B_\perp$, m | $H_a$, m | Event |
|---|---|---|---|---|---|---|
| 20 | 3051 | 1999/05/26 | 1999/03/17 | 74 | 107 | 1999/04/30 |
| 20 | 3051 | 1999/05/26 | 1999/04/21 | 99 | 80 | 1999/04/30 |
| 249 | 3051 | 1999/06/11 | 1999/04/02 | 5 | 1580 | 1999/04/30 |
| 478 | 3069 | 1999/04/18 | 1996/04/29 | 132 | 59 | 1997/05/05 |
| | | | | | | 1997/09/18 |
| 13 | 567 | 1999/05/25 | 1997/10/06 | 71 | 111 | 1998/10/01 |
| 392 | 3051 | 1998/09/14 | 1996/05/27 | 74 | 107 | unknown |
| 392 | 3051 | 1999/03/08 | 1996/05/28 | 124 | 64 | unknown |

cataloged earthquakes (Tables 1 and 2, Figure 2). In addition, we observe a region of uplift that is not associated with any earthquake in the seismic catalogs, or any topography that could induce an elevation-dependent atmospheric effect. We observe this deformation feature with the same magnitude in two independent interferograms that span different overlapping time frames. Therefore
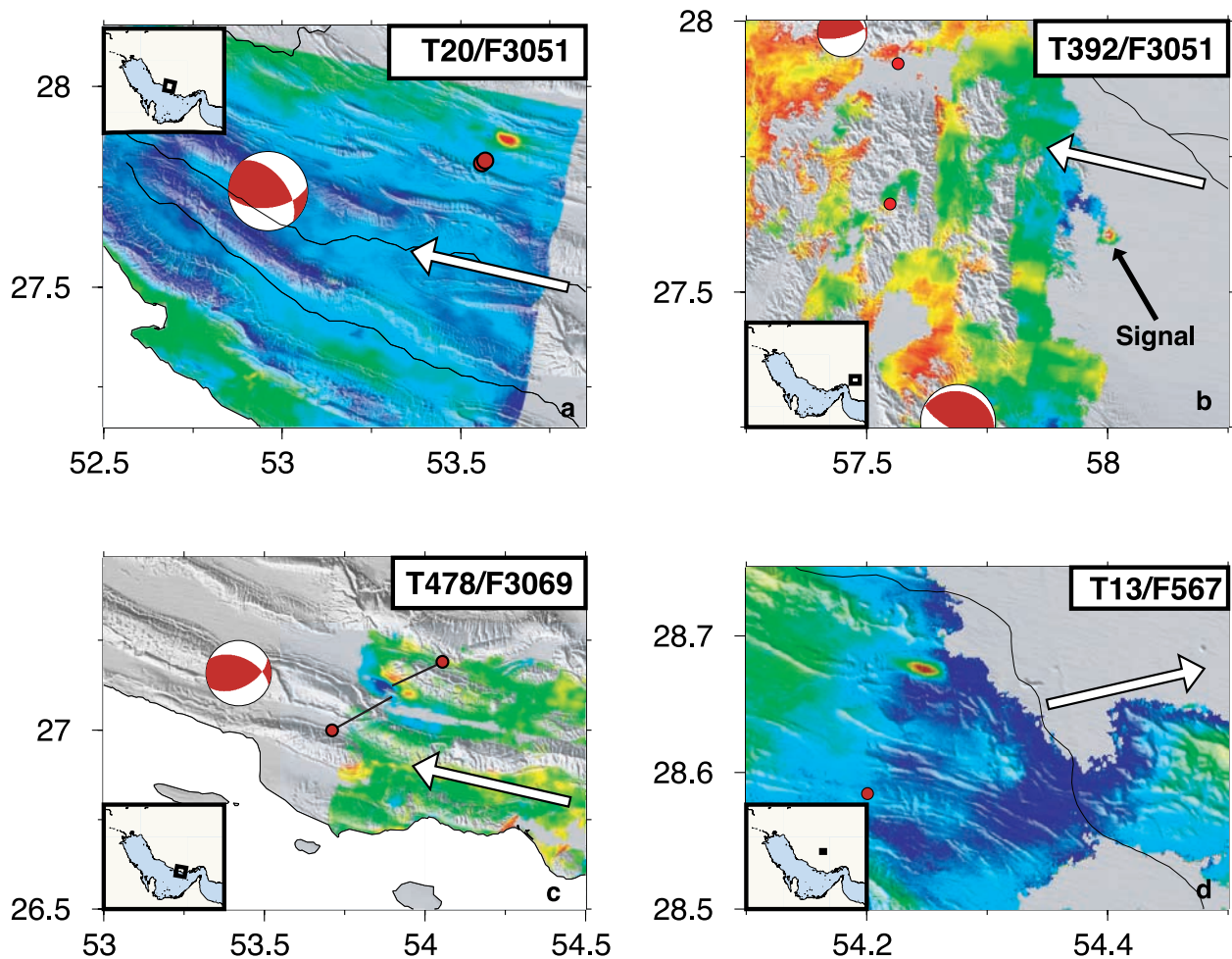


**Figure 2.** Summary of deformation sources. Interferograms for (a) the 1999/04/30 earthquake, (b) an unknown signal, (c) the 1997/05/05 and 1997/09/18 earthquakes, and (d) the 1998/10/01 earthquake, all overlain on topography, with the satellite-to-ground LOS direction indicated by the white arrow. Teleseismically determined locations for each inteferometric time interval (Table 2) are indicated by focal mechanisms (HCMT) and red circles (ISC). Note that both HCMT mechanisms are systematically to the west of the deformation observed in the InSAR data (Figures 2a and 2c). ISC locations in Figure 2b are offset (black lines) so that they do not conceal the deformation field.

**Table 3.** Inversion Results: Source Parameters and 1σ Confidence Limits for Best Fit Point Sources, Finite Fault Patches, and Distributed Slip for Each Earthquake in Figure 2[a]

| Date | Type | $M_w$ | Z, km | Lon, deg | Lat, deg | Strike, deg | Dip, deg | Rake, deg | RMS, cm |
|---|---|---|---|---|---|---|---|---|---|
| 97/05/05 | Point | 5.4 | 5.2 ± 0.3 | 53.881 ± 0.3 km | 27.130 ± 0.3 km | 120* | 80 ± 4 | −90 ± 6 | 0.330 |
|  | Patch | 5.4 | 4.4 ± 0.3 | 53.882 ± 0.3 km | 27.128 ± 0.3 km | 120* | 80 ± 4 | −90 ± 5 | 0.326 |
|  | Dist. | 5.4 | 6.2 | 53.887 | 27.122 | 120* | 80* | −83 | 0.282 |
| 97/09/18 | Point | 5.0 | 3.5 ± 0.2 | 53.942 ± 0.2 km | 27.083 ± 0.2 km | 270* | 85 ± 6 | 91 ± 5 | 0.330 |
|  | Patch | 5.0 | 3.5 ± 0.2 | 53.942 ± 0.2 km | 27.084 ± 0.2 km | 270* | 85 ± 6 | 90 ± 6 | 0.326 |
|  | Dist. | 5.3 | 7.6 | 53.967 | 27.086 | 270* | 85* | 81 | 0.282 |
| 98/10/01 | Point | 4.5 | 1.4 ± 0.2 | 54.245 ± 0.3 km | 28.677 ± 0.1 km | 110* | 45 ± 5 | −61 ± 11 | 0.423 |
|  | Patch | 4.7 | 0.7 ± 0.1 | 54.250 ± 0.1 km | 28.679 ± 0.1 km | 110* | 51 ± 5 | −29 ± 16 | 0.409 |
|  | Dist. | 4.6 | 0.8 | 54.245 | 28.680 | 110* | 51* | −63 | 0.196 |
| 99/04/30 | Point | 5.3 | 4.1 ± 0.18 | 53.628 ± 0.25 km | 27.870 ± 0.22 km | 110* | 42 ± 6 | −85 ± 7 | 0.132 |
|  | Patch | 5.3 | 3.2 ± 0.15 | 53.630 ± 0.22 km | 27.871 ± 0.21 km | 110* | 53 ± 5 | −77 ± 13 | 0.051 |
|  | Dist. | 5.3 | 5.3 | 53.630 | 27.872 | 110* | 53* | −79 | 0.049 |
| Unknown | Point | 4.8 | 2.4 ± 0.2 | 57.995 ± 0.1 km | 27.613 ± 0.1 km | 150* | 45* | −146 ± 12 | 0.305 |
|  | Patch | 4.8 | 2.0 ± 0.2 | 57.995 ± 0.1 km | 27.613 ± 0.2 km | 150* | 45* | −147 ± 11 | 0.294 |
|  | Dist. | 4.8 | 2.2 | 57.997 | 27.603 | 150* | 45* | −103 | 0.208 |

[a] Location is to center of fault plane. Asterisks indicate values that were fixed during inversion. The error bounds on the rest of the mechanism would be larger by ∼10° if we did not fix these parameters, but the error bounds on depth would be only slightly altered.

we can constrain the timing of deformation to within a 26 month period, but cannot confidently associate this deformation with any one of the earthquakes spanned by this time interval (Figure 2b). We cannot rule out that this signal may be due to groundwater changes, although it is unlikely since the signal is so similar in both interferograms. We also note that both the 1999/04/30 and 1997/05/05 deformation signals are about 50km to the east of the HCMT locations, indicating a potential systematic bias of the HCMT locations of the sort often observed in remote regions.

[6] In cases where we did not observe the earthquake deformation that we expected, the most common cause is widespread decorrelation across the interferogram. With a more complete InSAR data catalog, containing multiple interferometric pairs with short temporal baselines that spanned these earthquakes, it is likely that we would detect a higher percentage of the earthquakes. There are at least 13 cases of non-detection where we had a high-quality interferogram. In these cases, we infer that either the cataloged earthquake location is in error by more than ∼10−20 km, so that the earthquake actually occurred outside of the InSAR frame, or that the depth is great enough that the earthquake deformation is undetectable within the observed level of noise. For earthquakes of $M_w$ 4.5−5.0 and with only a single interferogram with noise levels similar to what we observe in this study, this critical depth ranges from approximately 5 to 15 km. We also checked for interferometric pairs in neighboring tracks and frames that would span each earthquake in case the cataloged location

was in error, but SAR coverage for this region is so sparse that no such data exist.

[7] We infer earthquake locations and magnitudes from the observed surface deformation using the Neighborhood Algorithm [*Sambridge*, 1998; *Lohman et al.*, 2002], a nonlinear inversion technique that employs a global search that focuses on regions with the lowest data misfit. Some of the factors that may contribute systematic errors to our result include atmospheric noise correlated with topography and the inhomogeneous elastic structure of the Earth. The locations and confidence intervals presented here do not account for variations in local elastic structure that may bias the inferred location and depth [e.g., *Du et al.*, 1997; *Savage*, 1998; *Masterlark*, 2003; *Zhao et al.*, 2004]. From the results *Lohman et al.* [2002], we expect that the main effect of rheological differences is to move the apparent depth by ∼10%. In addition, each interferogram may include aseismic deformation, such as postseismic slip. In one case, our data span two earthquakes (T478 interferogram), so we simultaneously search for two separate fault planes.

[8] We invert for the best fitting point sources and for the best fitting finite fault patches for each earthquake (Tables 1−3). For all the earthquakes discussed here, we only have interferograms from one satellite line-of-sight (LOS) direction. A single component of deformation provides little constraint on the mechanisms of small earthquakes [e.g., *Lohman et al.*, 2002], and complications such as spatially complex slip distributions, shallow after-
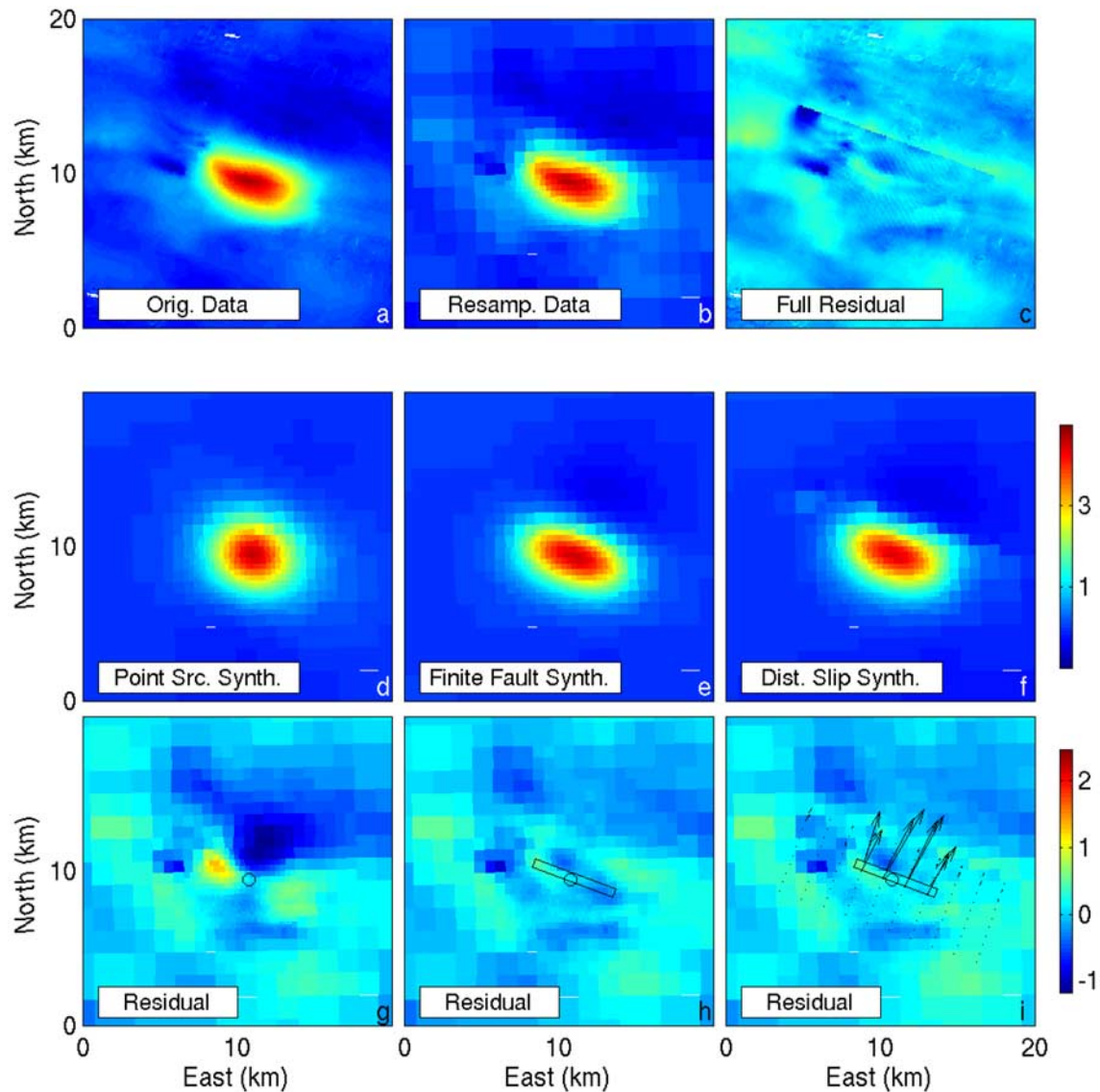
**Figure 3.** Inversion results for 1999/04/30 earthquake (T20/F3051): (a) Full data set, (b) resampled data used in inversion, and (c) full data residual using model in Figure 3i. (d–f) Synthetics and (g–i) data residuals for best point source, finite fault patch, and slip distribution, with color bar on right indicating LOS deformation in centimeters. The best fitting source geometry is indicated for each case. Arrows indicate slip vectors for distributed slip inversion in Figure 3i. Point source and finite fault patch geometries are included in Figures 3g and 3h for reference. Note that the centroid of slip in Figure 3i agrees with the location of the best fitting single fault patch. Color scales in Figures 3a and 3b are the same as in Figures 3d–3f, and color in Figure 3c is the same as in Figures 3g–3i.

shocks and correlated atmospheric noise can result in inferred mechanisms that are at odds with the regional structural trends and local seismicity. Therefore we infer the best fitting hypocentral locations with the strike constrained to agree in general with mechanisms in the existing seismic catalogs and with the surrounding structural trends (asterisks in Table 3). For instance, the 1997/05/05 event is associated with the axis of a syncline and it's near-vertical dip would be consistent with shallow faulting along the syncline core. In the case of the unknown signal, which is almost perfectly radially symmetric, we cannot rely on the simple structural trends that are found in the central Zagros. We fix the strike and dip mainly because the inversion would otherwise take a very long time to converge. No value should be attached to the mechanism for the unknown event, but the hypocenter and magnitude estimates are fairly robust.
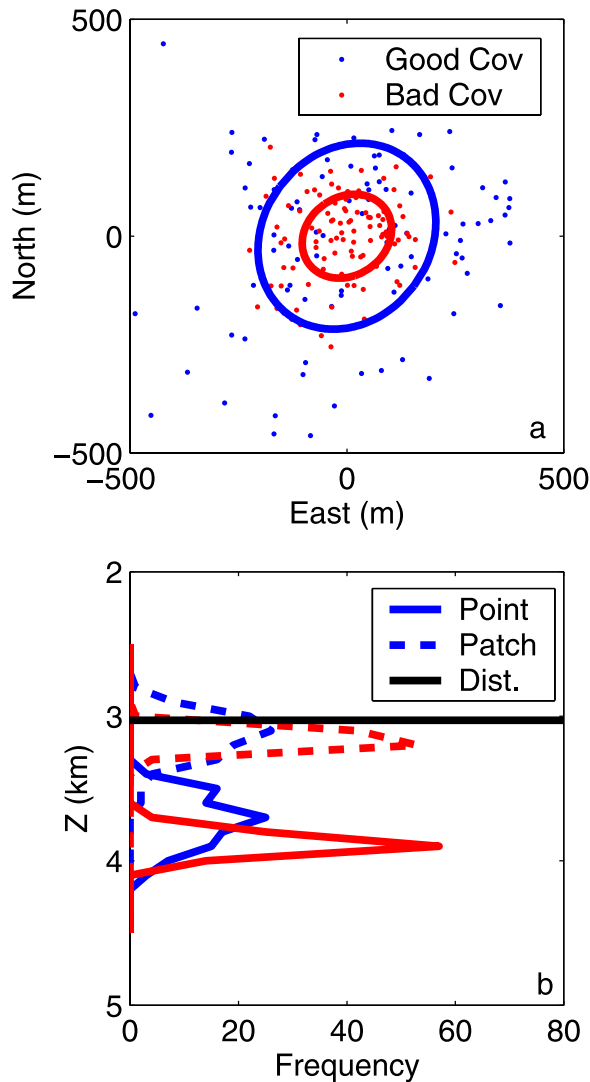
**Figure 4.** Results of a Monte Carlo sensitivity test for the 1999/04/30 earthquake: (a) Inferred map view locations of best fitting finite fault patch for each realization of a synthetic noisy data set (dots) using the full noise covariance (blue) and just the diagonal of the covariance (red). Ellipses indicate the 1σ error bounds on the inferred location (Table 3). (b) Histogram of inferred depths from Monte Carlo sensitivity test for point source (solid lines) and single finite fault patch inversions (dashed lines), with colors corresponding to noise covariance as in Figure 4a. Black line indicates the centroid of slip from the distributed slip inversion, which agrees well with the single finite fault patch inversion results.

[9] For each earthquake, we perform Monte Carlo error analyses on the hypocenter locations using the full noise covariance matrix. We create 100 synthetic data sets using the best fitting single finite fault patch and slip model for each earthquake (Table 3) and correlated noise using the

noise covariance estimated directly from the data [*Lohman and Simons*, 2005]. We invert each synthetic data set without fixing the fault plane geometry or mechanism in order to achieve more conservative error bounds.

[10] Synthetic data and residuals for the best models for the 1999/04/30 earthquake are shown in Figure 3, with 1σ error bounds on the inferred earthquake parameters tabulated in Table 3. The use of precise earthquake locations, such as in the Comprehensive Nuclear Test Ban Treaty (CTBT) program, requires accurate confidence intervals on earthquake hypocenters and magnitudes that include the contribution from data noise. We compare the Monte Carlo inversion results using the full noise covariance matrix with inversions only the diagonal of the noise covariance (i.e., no spatial correlation) in Figure 4. When the noise is correlated, there is effectively less information in the inversion and the data place weaker constraints on the model parameters. Thus the error bounds we place on our inferred location are larger when we include spatial covariance of the noise [e.g., *Lohman and Simons*, 2005]. See Figure 5.

[11] As can be seen in Figures 3g and 3h, the data for the 1999/04/30 earthquake are not adequately fit by either a point source or single fault patch. Because these earthquakes are so shallow, they warrant inversions allowing for distributed fault slip in order to more completely characterize the earthquake. For each earthquake, we expanded the best fitting finite fault patch and divided it into $10 \times 10$ smaller fault patches. We invert the InSAR data for the best fitting slip distribution, with smoothing constraints imposed using the $_jR_i$-criterion described by R. Lohman and M. Simons (Inferring fault slip from surface deformation using a spatially variable regularization scheme, submitted to *Geophysical Journal International*, 2004). Note that the centroid of slip (arrows) agrees with the location of the best fitting single fault patch and that the fit only improves slightly.

[12] For all four earthquakes (Figures 3, 6, and 7), the InSAR-derived magnitude is consistently larger than the magnitude from either seismic catalog (Table 1). This may be due in part to the fact that neither we nor the seismic catalogs use a realistic layered rheology, which affects the inferred seismic moment. Also, each interferogram potentially includes postseismic deformation and aftershocks in addition to the mainshock. Therefore each location should be viewed as a centroid for the
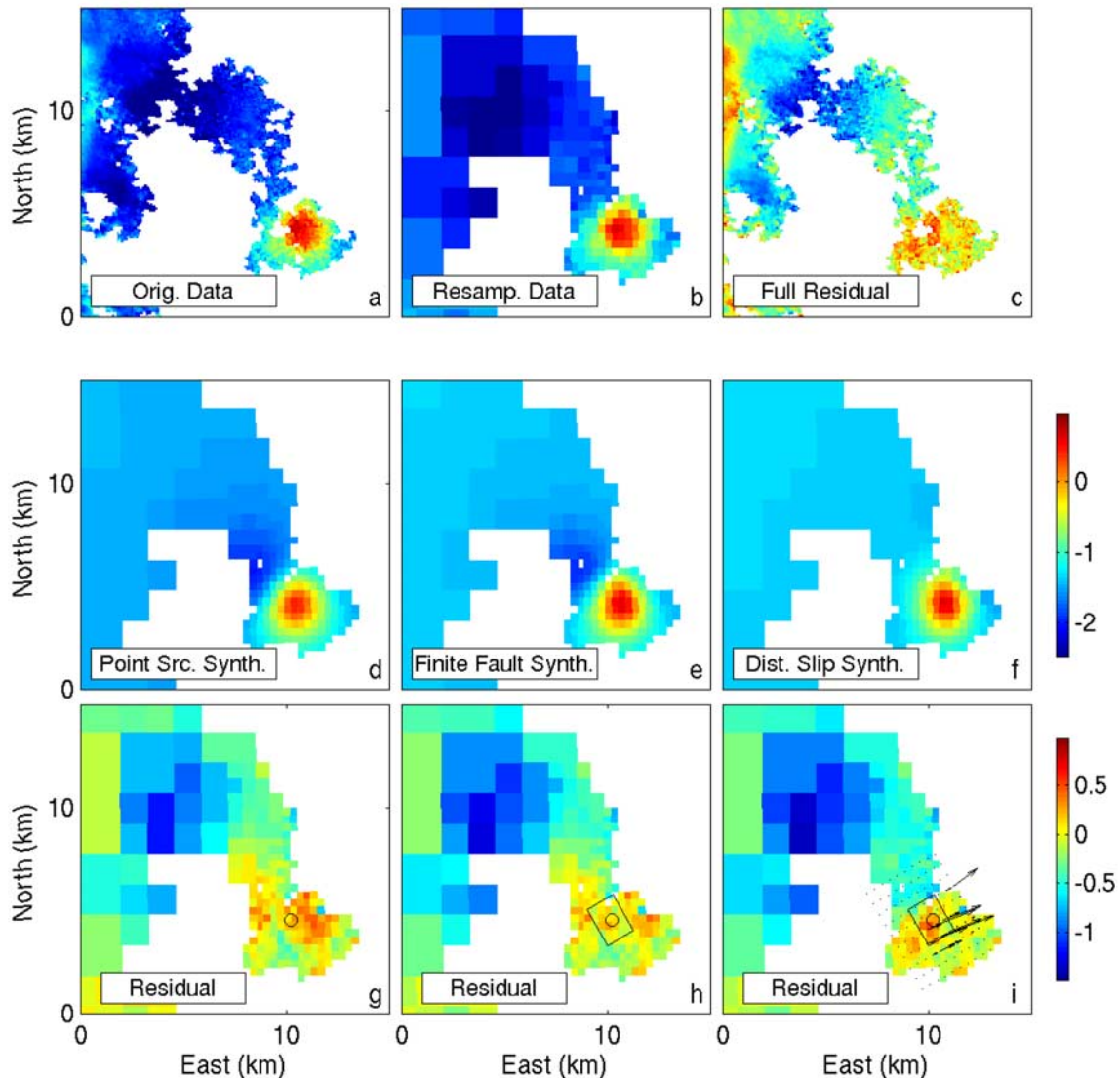
**Figure 5.**   Inversion results for unknown signal (T392/F3051). Panels as in Figure 3.

deformation that occurred during that time period. Again, here we are limited by the time resolution of the available InSAR data.

## 4. Conclusions

[13]  The type of analyses presented here contribute to the creation of a geodetically derived earthquake catalog complementing existing teleseismically determined catalogs. The InSAR data allow us to precisely locate earthquakes that are too small to be well-located by either the HCMT or ISC catalogs. With only a single LOS component of deformation, we have little information about the mechanism of the earthquake, but can determine the location with a precision of a few kilometers

in map view and depth. Precise earthquake locations such as these can be inputs into tomographic models or tectonic studies that have previously been limited by our knowledge of the distribution of seismicity. Southern Iran is an ideal candidate for an InSAR-derived catalog, as it has a high level of seismicity and a relatively sparse local seismic network.

[14]  This work was seriously hampered by the limited SAR data coverage in southern Iran. In most cases, the interferogram time periods were so long that it was not possible to associate observed deformation with a specific earthquake, or to distinguish earthquakes that occurred in clusters. The long time periods also resulted in widespread decorrelation, inhibiting us from placing minimum
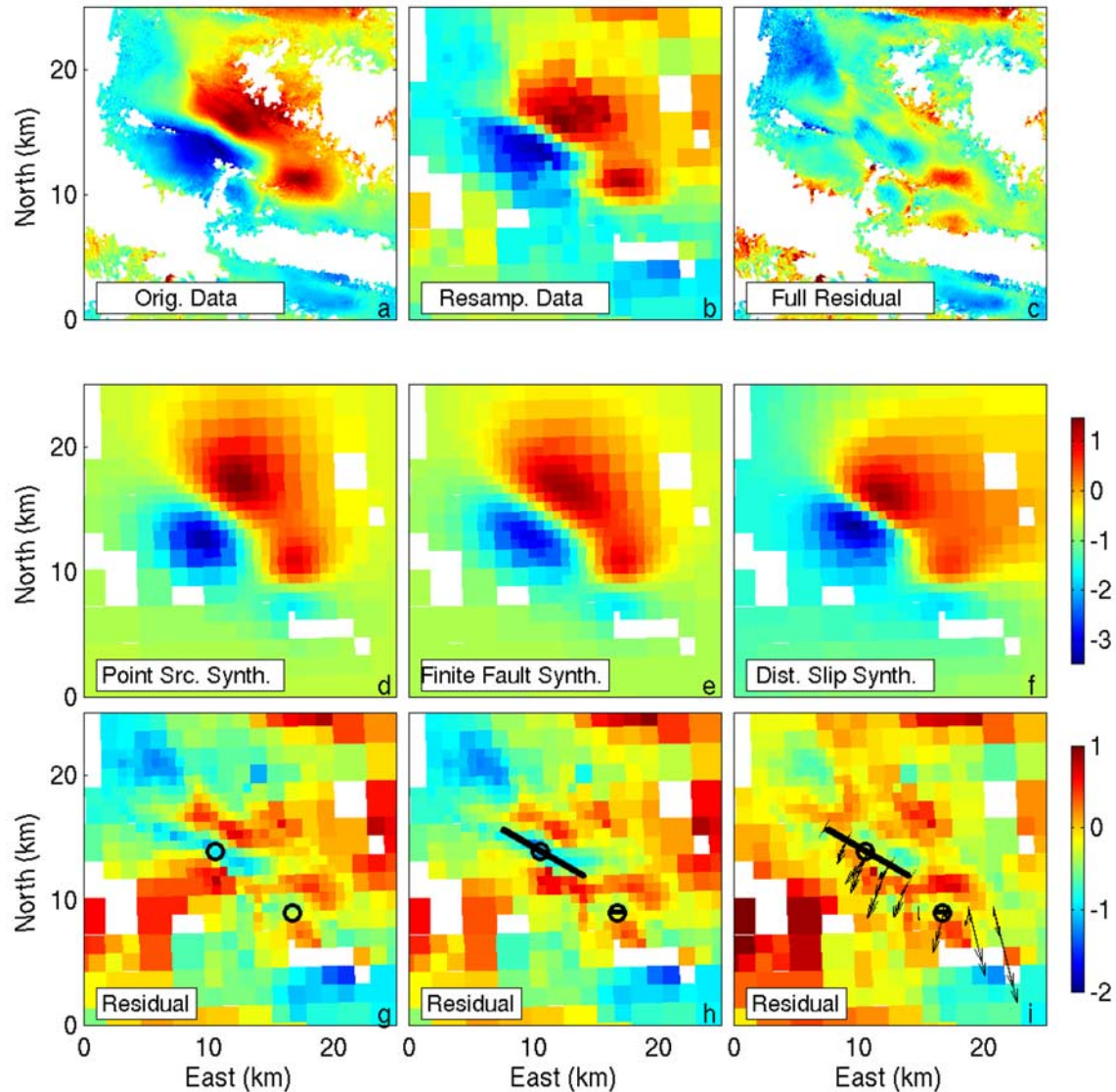
**Figure 6.** Inversion results for 1997/05/05 and 1997/09/18 earthquakes (T478/F3069). Panels as in Figure 3. The fault planes are nearly vertical.

depth constraints on the earthquakes we examined, since we would not have detected them even if they were shallow. A dedicated satellite system providing increased spatial and temporal data coverage would greatly facilitate this type of study. Given the noise levels we observe in interferograms for southern Iran, we can expect to detect $M_w$ 4 and 5 earthquakes that are shallower than around 5 km and 15 km, respectively, whenever the interferograms are otherwise of good quality (i.e., good correlation and limited topographic artifacts). When multiple interferograms are available that span the same earthquake, we can stack the data to reduce the signal to noise ratio and potentially observe smaller and/or deeper events.

[15] In this study, we sought to determine whether earthquake locations in the Zagros mountains were consistent with a deformation regime dominated by basement faulting, or if seismicity occurs throughout the crustal section. Because of the limitations described above, we are far from a complete catalog of seismicity and can draw no conclusions about what percentage of seismicity occurs in the basement rocks. However, the earthquakes discussed here are all in the upper few km of the crust, so at least some deformation may be accommodated seismically within the sedimentary section. The InSAR locations that we find can also be used to help calibrate seismic models for the region, which will help seismologists determine if
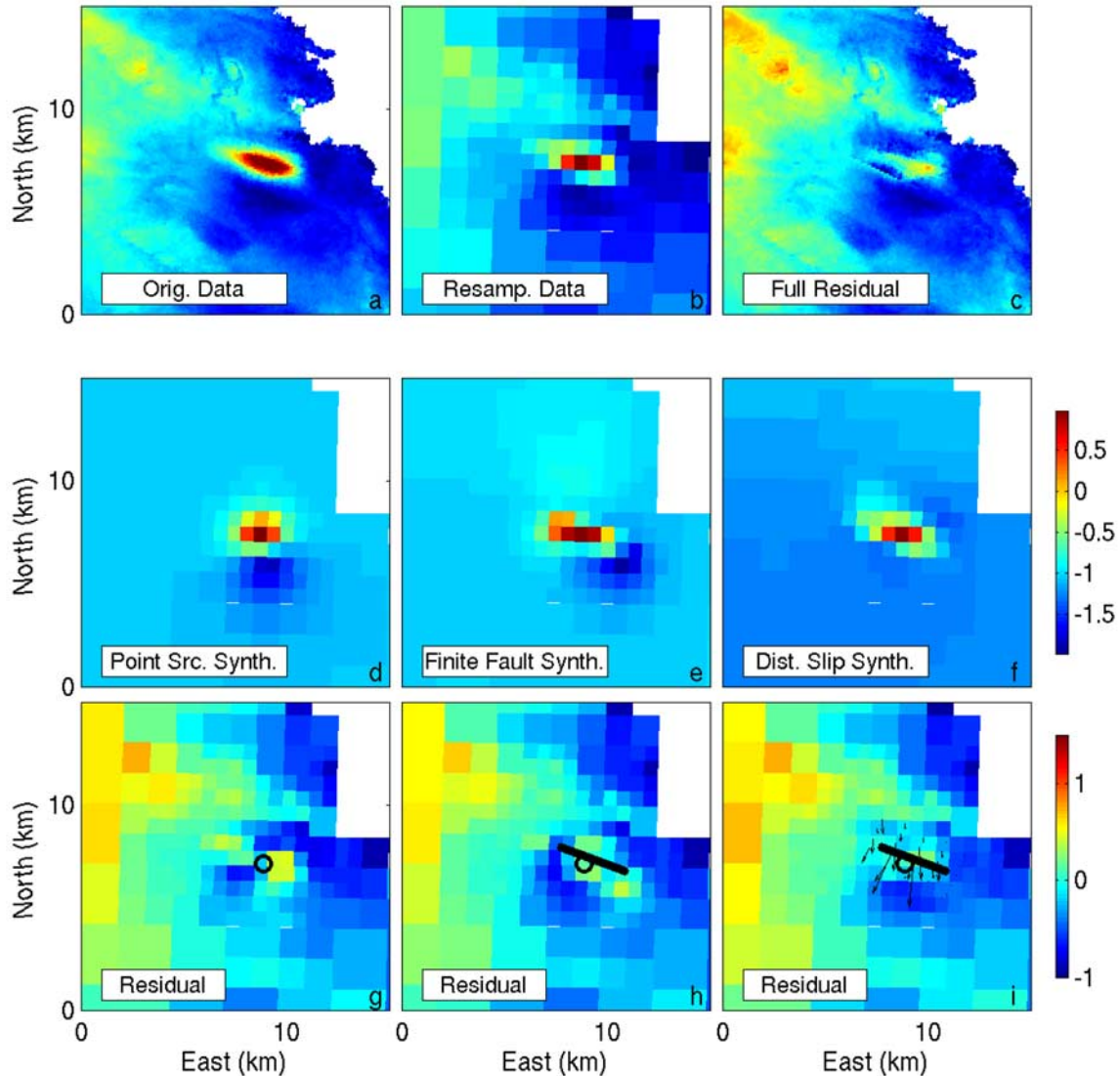
**Figure 7.** Inversion results for 1998/10/01 earthquake (T13/F567). Panels as in Figure 3. The inferred fault plane has a greater along-strike length than down-dip extent, resulting in the narrow appearance of the fault in Figure 7h.

earthquakes that are too small and deep to resolve with InSAR truly occur in the basement.

## Acknowledgments

## References

Ambraseys, N. N. (2001), Reassessment of earthquakes, 1900–1999, in the Eastern Mediterranean and the Middle East, *Geophys. J. Int.*, *145*, 471–486.

DeMets, C., R. G. Gordon, D. F. Argus, and S. Stein (1994), Effect of recent revisions to the geomagnetic reversal time scale on estimates of current plate motions, *Geophys. Res. Lett.*, *21*, 2191–2194.

Du, Y., P. Segall, and H. J. Gao (1997), Quasi-static dislocations in three dimensional inhomogeneous media, *Geophys. Res. Lett.*, *24*, 2347–2350.

Farr, T. G., and M. Kobrick (2000), Shuttle Radar Topography Mission produces a wealth of data, *Eos Trans. AGU*, *81*(48), 583–585.

Hessami, K., H. A. Koyi, and C. J. Talbot (2001), The significance of strike-slip faulting in the basement of the Zagros fold and thrust belt, *J. Pet. Geol.*, *24*, 5–28.

Jackson, J., and T. J. Fitch (1981), Basement faulting and the focal depths of the larger earthquake in the Zagros mountains (Iran), *Geophys. J. R. Astron. Soc.*, *64*, 561–586.

Jackson, J., and D. McKenzie (1988), The relationship between plate motions and seismic moment tensors, and the rates of active deformation in the Mediterranean and Middle East, *Geophsy. J. Int.*, *93*, 45–73.

Lohman, R. B., and M. Simons (2005), Some thoughts on the use of InSAR data to constrain models of surface deformation: Noise structure and data downsampling, *Geochem. Geophys. Geosyst.*, *6*, Q01007, doi:10.1029/2004GC000841.

Lohman, R. B., M. Simons, and B. Savage (2002), Location and mechanism of the Little Skull Mountain earthquake as constrained by satellite radar interferometry and seismic waveform modeling, *J. Geophys. Res.*, *107*(B6), 2118, doi:10.1029/2001JB000627.

Maggi, A., J. A. Jackson, K. Priestley, and C. Baker (2000), A re-assessment of focal depth distributions in southern Iran, the Tien Shan and northern India: Do earthquakes really occur in the continental mantle?, *Geophys. J. Int.*, *143*, 629–661.

Masterlark, T. (2003), Finite element model predictions of static deformation from dislocation sources in a subduction zone: Sensitivities to homogeneous, isotropic, Poisson-solid, and half-space assumptions, *J. Geophys. Res.*, *108*(B11), 2540, doi:10.1029/2002JB002296.

Rosen, P. A., S. Hensley, I. R. Joughin, F. K. Li, S. N. Madsen, E. Rodriguez, and R. M. Goldstein (2000), Synthetic aperture radar interferometry, *Proc. IEEE*, *88*, 333–382.

Rosen, P. A., S. Hensley, G. Peltzer, and M. Simons (2004), Updated repeat orbit interferometry package released, *Eos Trans. AGU*, *85*(5), 47.

Sambridge, M. (1998), Geophysical inversion with a neighborhood algorithm—I, Searching a parameter space, *Geophys. J. Int.*, *138*, 479–494.

Savage, J. C. (1998), Displacement field for an edge dislocation in a layered elastic half-space, *J. Geophys. Res.*, *103*, 2439–2446.

Talebian, M., and J. Jackson (2004), A reappraisal of earthquake focal mechanisms and active shortening in the Zagros mountains of Iran, *Geophys. J. Int.*, *156*, 506–526.

Zhao, S., R. D. Muller, Y. Takahashi, and Y. Kaneda (2004), 3-D finite-element modelling of deformation and stress associated with faulting: Effect of inhomogeneous crustal structures, *Geophys. J. Int.*, *157*, 629–644.